Robust Design of Independent Joint Controllers with Experimentation on a High-Speed Parallel Robot

Pasquale Chiacchio, François Pierrot, Lorenzo Sciavicco, and Bruno Siciliano, *Member, IEEE*

Abstract—**The dynamic model of a robot manipulator is described by a set of nonlinear, highly coupled differential equations. Model-based control schemes were proposed to enhance tracking capabilities with respect to simple linear control schemes. Independent joint controllers (of PD or PID type) are usually employed in industrial robot manipulators but cannot achieve satisfactory performance due to their inherent low rejection to disturbances and parameter variations. In this paper, a new linear independent joint control scheme is proposed; the design is made robust by closing another feedback loop that uses acceleration information besides the typical position and velocity loops. Reconstruction of acceleration measurements is performed via a suitable state-variable filter. Linear feedforward compensation is used to improve tracking performance of the closed-loop scheme. The control algorithm is tested first in a discrete-time simulation on a single-joint drive system with imposed disturbance torques. Then real-time implementation on a high-speed parallel robot is presented; the experimental results demonstrate the effectiveness of the proposed technique.**

I. Introduction

It is well known that the dynamic model of a robot manipulator is described by a set of nonlinear, highly coupled differential equations. In view of this, model-based control algorithms were proposed that have a potential for performance improvement over the independent joint controllers that do not account for manipulator dynamics [1], e.g., PD or PID type as in current industrial robots. A model-based control design compensates for the available estimates of the dynamic terms in a feedback or in a feedforward fashion, and a linear feedback loop provides robustness to imperfect modeling and unavoidable disturbances. The computed torque control, which performs dynamic compensation in a feedback [2] or in a feedforward fashion [3], was the pioneer design of this kind; nevertheless, a large number of control schemes can be conceived under this class [4], including adaptive control algorithms that exploit model information [5]–[7].

Early experimental investigation of model-based control algorithms was addressed to research laboratory manipulators having direct-drive actuators [8], for which dynamic terms do play an important role in robot high-speed motion [9], [10]. Later, however, it was demonstrated that also for industrial robots with high gear ratios dynamic compensation yields significant reduction of tracking errors [11], [12]. The effects of variable payloads [13], and of drive system and asynchronous dynamic compensation [14] were extensively studied for a PUMA-560 robot arm.

In spite of all the foregoing nice features, model-based control relies all its potential on the correctness and completeness of dynamic models that are just idealizations of the physical components of the robot, i.e., the manipulator, the actuators, the joint transmission, the transducers, etc. For this reason, we believe that the design of linear compensators for each joint servo is still a valid alternative to model-based control, on condition that effective rejection of disturbance torques is achieved.

A new robust independent joint control scheme is proposed in this work, originated from the preliminary study in [15]. The design takes advantage of an acceleration feedback loop in addition to the conventional position and velocity loops used for control of servomechanisms. The scheme allows the setting of desired disturbance rejection factor and recovery time. A state-variable filter is utilized for reconstructing acceleration measurements.

Similar research efforts were produced in [16], [17] that demonstrated the effectiveness of this approach; recently, the scheme proposed in [16] was also experimentally tested [18] and showed comparable performance to that of a computed torque control. Alternatively, a scheme that makes use of acceleration information to estimate and compensate the nonlinear and coupling terms was recently presented in [19]. All these schemes, however, exploit model knowledge to perform an indirect feedforward compensation of the nonlinear terms. Our scheme, instead, is entirely based on a linear control design that takes advantage of acceleration feedback and treats all the nonlinearities as a disturbance.

To show the potential of the proposed control design, discrete-time simulation tests were carried out for a

Manuscript received March 6, 1992; revised December 4, 1992. This work was supported partly by the Consiglio Nazionale delle Ricerche under Contract 92.01064.PF67, and partly by Commission of the European Communities under an ESPRIT Research Grant assigned to P. Chiacchio to support his stay at LIRMM.

P. Chiacchio, L. Sciavicco, and B. Siciliano are with the Dipartimento di Informatica e Sistemistica, Università degli Studi di Napoli Federico II, 80125 Napoli, Italy.

F. Pierrot is with the Laboratoire d'Informatique, de Robotique et de Microélectronique de Montpellier, Université Montpellier II, 34392 Montpellier Cedex 5, France.

IEEE Log Number 9209258.

single-joint drive system with both step and sinusoidal imposed disturbance torques. Then, the scheme was implemented in real time on a multitransputer system controlling the high-speed parallel robot DELTA [20]. Even if the robot is very light, the nonlinear and coupling dynamical terms cannot be considered negligible [21] since it is capable to perform high-speed and high-acceleration motion; this is due also to the fact that, in the laboratory prototype, the gear ratio is only 1 : 10. Experimental results are described with different sampling rates and compared with those of a classical PID controller.

The paper is organized as follows. Section II gives the background of independent joint space control based on the usual position + velocity feedback scheme. Section III proposes the new robust control scheme with acceleration feedback that guarantees prescribed disturbance rejection and allows trajectory tracking. The results of simulation tests are presented in Section IV. An extensive description of the experimental results is provided in Section V. Conclusions are drawn in Section VI.

II. Independent Joint Control

The problem of controlling the motion of a servomanipulator is that to determine the history of generalized forces (linear forces or torques) to be applied at the joint actuators in order to guarantee the execution of an assigned trajectory, according to certain requirements on transient and steady state.

The dynamic model of a robotic manipulator in free space is described by the equation of motion

$$\boldsymbol{B}(\boldsymbol{q})\ddot{\boldsymbol{q}} + \boldsymbol{n}(\boldsymbol{q}, \dot{\boldsymbol{q}}) = \boldsymbol{\tau} \tag{1}$$

where $\boldsymbol{q}$ is the $(n \times 1)$ vector of joint variables, $\boldsymbol{B}$ is the $(n \times n)$ positive definite symmetric inertia matrix, $\boldsymbol{n}$ is the $(n \times 1)$ vector accounting for all the other dynamic effects, e.g., Coriolis and centrifugal forces, friction forces, gravitational forces, and $\boldsymbol{\tau}$ is the $(n \times 1)$ vector of joint driving forces.

To control the motion of the manipulator means to determine the forces $\boldsymbol{\tau}$ that allow the execution of a motion $\boldsymbol{q}(t)$, such that it closely be

$$\boldsymbol{q}(t) = \boldsymbol{q}_d(t)$$

where $\boldsymbol{q}_d(t)$ indicates the vector of reference joint variables.

The joint forces are provided by the actuators via kinematic transmissions that perform a motion transformation from the motors to the links. If $\boldsymbol{q}_m$ is the $(n \times 1)$ vector of actuator displacements, the following relation is obtained

$$\boldsymbol{K}_r\boldsymbol{q} = \boldsymbol{q}_m \tag{2}$$

where $\boldsymbol{K}_r$ is an $(n \times n)$ diagonal matrix of gear reductions; the entries of $\boldsymbol{K}_r$ are much greater than unity for typical gear-driven industrial robots.

In view of (2), the vector of actuator driving forces $\boldsymbol{\tau}_m$ is given by

$$\boldsymbol{\tau}_m = \boldsymbol{I}_m\ddot{\boldsymbol{q}}_m + \boldsymbol{F}_m\dot{\boldsymbol{q}}_m + \boldsymbol{K}_r^{-1}\boldsymbol{\tau} \tag{3}$$

where $\boldsymbol{I}_m$ and $\boldsymbol{F}_m$ are diagonal matrices whose elements are the inertias and viscous friction coefficients of the gear reduction motors, and $\boldsymbol{K}_r^{-1}\boldsymbol{\tau}$ is the vector of required joint torques resulting at the actuator axes.

At this point, observing that the diagonal elements of the inertia matrix contain constant terms, which do not depend on the joint configuration, and configuration-dependent terms (combination of sinusoidal functions), $\boldsymbol{B}(\boldsymbol{q})$ can be decomposed as

$$\boldsymbol{B}(\boldsymbol{q}) = \bar{\boldsymbol{B}} + \Delta\boldsymbol{B}(\boldsymbol{q}) \tag{4}$$

where $\bar{\boldsymbol{B}}$ is a diagonal matrix whose constant elements represent the average values of joint inertias. Plugging (1), (2), and (4) into (3) gives

$$\boldsymbol{\tau}_m = \left(\boldsymbol{I}_m + \boldsymbol{K}_r^{-1}\bar{\boldsymbol{B}}\boldsymbol{K}_r^{-1}\right)\ddot{\boldsymbol{q}}_m + \boldsymbol{F}_m\dot{\boldsymbol{q}}_m + \boldsymbol{d} \tag{5}$$

where

$$\boldsymbol{d} = \boldsymbol{K}_r^{-1}\Delta\boldsymbol{B}\boldsymbol{K}_r^{-1}\ddot{\boldsymbol{q}}_m + \boldsymbol{K}_r^{-1}\boldsymbol{n} \tag{6}$$

is the actuator torque accounting for all the (nonlinear) coupling terms. It is understood that $\boldsymbol{d}$ can include also any model uncertainty of system components.

As evidenced by the block diagram scheme of Fig. 1, the servosystem is actually composed of two subsystems; one with $\boldsymbol{\tau}_m$ as input and $\boldsymbol{q}_m$ as output, the other with $\boldsymbol{q}_m, \dot{\boldsymbol{q}}_m, \ddot{\boldsymbol{q}}_m$ as input and $\boldsymbol{d}$ as output. The former is *linear* and *decoupled*; each component of $\boldsymbol{\tau}_m$ affects the corresponding component of $\boldsymbol{q}_m$. The latter is *nonlinear* and *coupled*, since it accounts for all those nonlinear and interacting contributions stemming from the joint coupled dynamics.

On the basis of the foregoing scheme, a large variety of control algorithms can be devised with respect to the required accuracy of dynamic model knowledge. The simplest approach to follow, in the case of high gear ratios and/or of low operational speeds, is to regard $\boldsymbol{d}$ as a vector of *disturbance* forces for the joint servos. This corresponds to a *decentralized* structure of the controller, since each joint is controlled independently from the others. The design of the control algorithm must guarantee high performance in terms of *disturbance rejection* and *trajectory tracking*. The system to control is the servo of the ith joint of the manipulator; hereafter, all the quantities are referred to the single joint drive system.

It is supposed that dc or brushless motors are employed. Electrical motor drives can be either voltage or current controlled; in robotic applications, they are typically current controlled so that the drive system behaves as an ideal torque generator. No matter which control mode is

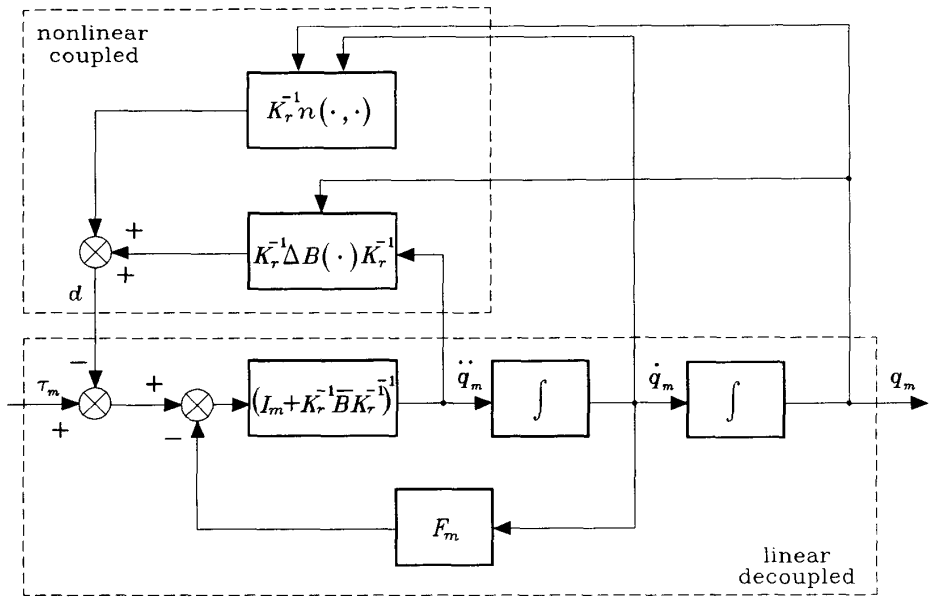

Fig. 1. Block diagram scheme of the dynamics of a robot manipulator.

used, the servo can be described by the second-order transfer function

$$M(s) = \frac{k_m}{s(1 + sT_m)} \tag{7}$$

where k_m and T_m are the gain and the time constant, respectively. Their values depend on the motor physical parameters and the kind of control. The transfer function (7) describes the relation between the input (either voltage or current) and the output (position).

An effective rejection of the component of the disturbance torque $\boldsymbol{d}$ acting on the single joint is ensured by a PI action for the controller, yielding zero error at steady state for a step disturbance and offering a stabilizing effect. Besides the closure of a position feedback loop, the typical solution used for control of servomechanisms is to close a feedback velocity loop. Notice that the above disturbance can be reported at the input of each servo as either a disturbance voltage or a disturbance current; let d' denote such disturbance.

Classical feedback control theory suggests to place the zero of the regulator at $s = -1/T_V$ to cancel the effects of the real pole of the motor at $s = -1/T_m$, i.e., $T_V = T_m$, to obtain the typical second-order closed-loop input/output transfer function

$$\frac{Q(s)}{Q_d(s)} = \frac{1}{1 + \dfrac{s}{K_P} + \dfrac{s^2}{k_m K_P K_V}} \tag{8}$$

where Q_d denotes the reference input. Hence, if the natural frequency ω_n and the damping ratio ζ are given as design requirements, the following relations can be established:

$$K_V = \frac{2\zeta\omega_n}{k_m} \tag{9}$$

$$K_P K_V = \frac{\omega_n^2}{k_m}. \tag{10}$$

Once K_V has been chosen to satisfy (9), the value of K_P is obtained from (10).

Furthermore, the closed-loop disturbance/output transfer function is

$$\frac{Q(s)}{D'(s)} = -\frac{\dfrac{s}{K_P K_V(1 + sT_V)}}{1 + \dfrac{s}{K_P} + \dfrac{s^2}{k_m K_P K_V}} \tag{11}$$

which shows that the term $K_P K_V$ is the reduction factor imposed by the feedback gains on the amplitude of the output due to the disturbance; then, the quantity

$$X_R = K_P K_V \tag{12}$$

can be interpreted as the disturbance rejection factor and is fixed, once K_P and K_V have been chosen via (9), (10). Concerning the disturbance dynamics, an estimate of the disturbance recovery time is given by the time constant

$$T_R = \max\left\{T_m, \frac{1}{\zeta\omega_n}\right\}. \tag{13}$$

In (11), the zero in the origin introduced by the PI allows to counteract the effects of gravity in D' at steady state.

The resulting scheme is illustrated in Fig. 2, which also shows the presence of a feedforward action both on

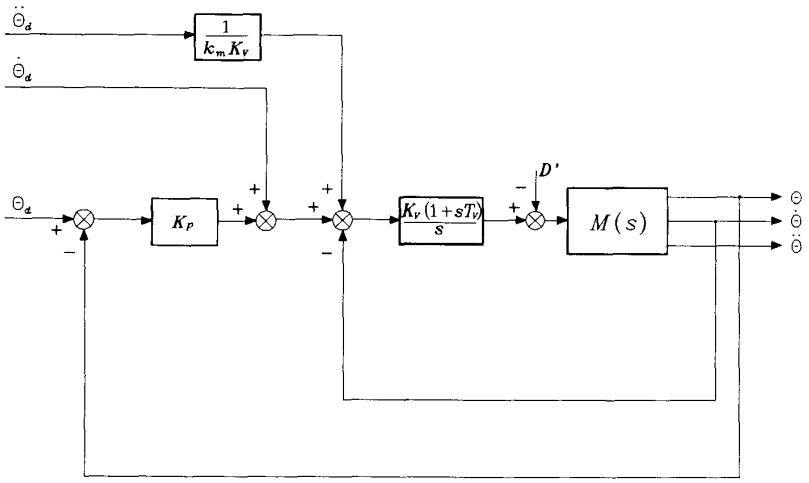

Fig. 2. Block diagram scheme of the P–PI independent joint control system.

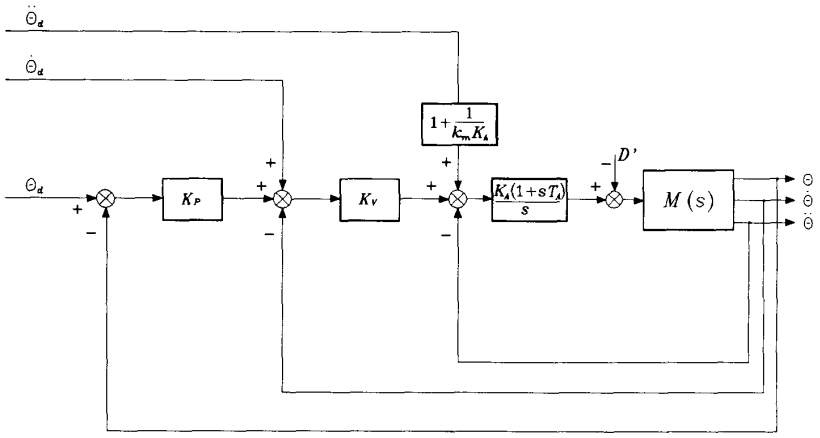

Fig. 3. Block diagram scheme of the P–P–PI independent joint control system.

velocity and acceleration [2]; this is aimed at canceling the plant dynamics and then enhance tracking of the desired joint position trajectory $q_d(t)$.

III. A New Robust Scheme with Acceleration Feedback

In order to allow the setting of desired values for the disturbance rejection factor and recovery time, the addition of an acceleration feedback loop is proposed as in the P–P–PI control scheme of Fig. 3. Interestingly enough, due to the presence of the inmost loop, it is now possible to set a limit on motor acceleration.

Notice that, differently from the previous case, the presence of the acceleration feedback does not allow to define the motor transfer function as in (7). The resulting transfer function of the equivalent feedback path is

$$(K_V + K_A)\left(1 + \frac{sK_A T_A}{K_V + K_A}\right).$$

At this point, the closed-loop transfer function of the inmost block is found to be

$$G'(s) = \frac{k_m}{(1 + k_m K_A)\left(1 + \dfrac{sT_m\left(1 + k_m K_A \dfrac{T_A}{T_m}\right)}{(1 + k_m K_A)}\right)}.$$

As a consequence, the overall transfer function of the forward path is

$$\frac{K_P K_V K_A (1 + sT_A)}{s^2} G'(s)$$

whereas that of the equivalent feedback path is

$$1 + \frac{s}{K_P}.$$

Also in this case, an opportune cancellation can be performed by setting

$$T_A = T_m$$

or

$$k_m K_A T_A \gg T_m \qquad k_m K_A \gg 1.$$

The two solutions are essentially the same, as far as the dynamic features of the control system are concerned. The second solution, however, permits to choose $T_A < T_m$.

The closed-loop input/output transfer function is

$$\frac{Q(s)}{Q_d(s)} = \frac{1}{1 + \dfrac{s}{K_P} + \dfrac{s^2(1 + k_m K_A)}{k_m K_P K_V K_A}}. \tag{14}$$

Moreover, the closed-loop disturbance/output transfer function is

$$\frac{Q(s)}{D'(s)} = -\frac{\dfrac{s}{K_P K_V K_A(1 + sT_A)}}{1 + \dfrac{s}{K_P} + \dfrac{s^2(1 + k_m K_A)}{k_m K_P K_V K_A}}. \tag{15}$$

The resulting disturbance rejection factor and recovery time are respectively given by

$$X_R = K_P K_V K_A \tag{16}$$

and

$$T_R = \max\left\{T_A, \frac{1}{\zeta\omega_n}\right\} \tag{17}$$

where T_A can be made less than T_m.

By comparison of (14) with the transfer function of a second-order system, the following relations can be established for design purposes:

$$2K_P = \frac{\omega_n}{\zeta} \tag{18}$$

$$1 + k_m K_A = \frac{k_m X_R}{\omega_n^2} \tag{19}$$

$$K_P K_V K_A = X_R. \tag{20}$$

Once K_P has been chosen to satisfy (18), K_A is chosen to satisfy (19), and then K_V is obtained from (20). Therefore, with respect to the previous case, now the acceleration feedback remarkably allows not only to achieve any desired dynamic behavior but also to prescribe the disturbance rejection factor.

Similarly to the case of the P–PI scheme, an enhancement of trajectory tracking is achieved by a feedforward compensation action, as shown in the scheme of Fig. 3.

It is important to stress that the foregoing derivation is based on reduced dynamic models, that is, neglecting the effects of joint elasticities, backlashes, and stiction; of amplifier and motor electrical time constants; and, in general, of any unmodeled dynamics. Other factors that influence the performance of the system are the discrete-time implementation of the controller, finite sampling times and sensor measurement noise. This implies that the fulfilment of design requirements by imposing high-gain constants for the compensator may not be verified in practice, leading to degraded performance and even to instability. An analytical discussion aimed at quantifying the above effects is difficult to carry out at this stage. Therefore, we postpone the treatment of practical implementation issues to the simulated case study in Section IV.

In deriving the foregoing control scheme, the issue of measurement of feedback variables was not considered explicitly. With reference to the typical position control servos that are implemented in industrial practice, there is no problem to measure position and velocity, while a direct measurement of acceleration in general either is not available or is too expensive to get. Therefore, for the scheme of Fig. 3, the acceleration measurement can be reconstructed from the position measurement by means of a state-variable filter (Fig. 4). The filter is characterized by a natural frequency $\omega_{nf} = \sqrt{k_1 k_2}$ and by a damping ratio $\zeta_f = (1/2)\sqrt{k_1/k_2}$. By choosing the filter bandwidth to be larger than the joint servo bandwidth—at least a decade off to the right—the effects due to measurement lags between q_f and q are not appreciable, and then it is feasible to take $\ddot{q}_f$ (and $\dot{q}_f$, if $\dot{q}$ is not available) as the quantity to feed back.

Finally, it must be remarked that the disturbance term is not completely unknown but an approximate expression is usually available. Therefore, it is understood that a model-based compensation can be performed—say in a feedforward fashion, to perform it off line for typically repetitive trajectories—which can alleviate the endeavor of disturbance rejection of the previous scheme. In other words, a valid solution from an engineering viewpoint could be that of devising the control system for a robot manipulator as composed of two subsystems—a decentralized robust independent joint control with acceleration feedback whose performance can be enhanced by the introduction of a centralized model-based (feedforward) control that compensates for the relevant contributions of manipulator dynamics.

IV. Simulation Tests

In order to test the performance of the P–P–PI scheme compared to that of the classical P–PI scheme, a set of simulation tests were carried out. The software package SIMNON was utilized to simulate the control algorithm in discrete time with a sampling time of 1 ms.

A single-joint voltage-controlled drive system was considered and disturbance torques were added to simulate the effect of coupling arising from other joints. The motor is an AXEM MD 15 HS; its parameters are $k_t = 0.248$ N/A, $k_v = 0.248$ V/s, $R_a = 1.25\ \Omega$, $F_m = 0.001$ N · s/rad, $I_m = 0.000423$ kg · m^2 (including the load). These data lead to the transfer function of the kind

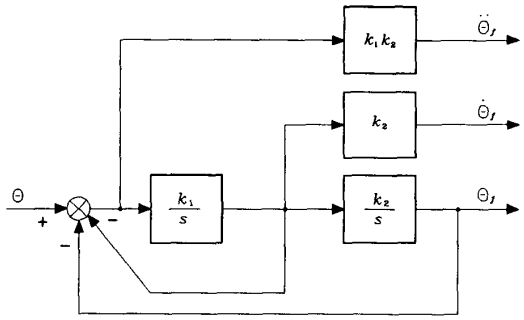

Fig. 4. Block diagram scheme of the state variable filter.

in (7)

$$M(s) = \frac{4.03}{s(1 + 0.0172s)}.$$

A 10% variation of the inertia load was always added in the simulated model with respect to the foregoing nominal model used for control design.

Saturation limits were set to 10 A on the current and to 100 V on the voltage. Furthermore, to simulate a situation close to reality, also the dynamics of the power amplifier was included in simulation via the transfer function

$$A(s) = \frac{1}{1 + 0.005s}.$$

The feedback gains of the two controllers were chosen so that the same dynamic behavior is obtained in both cases and a comparison be significant. In particular, a natural frequency $\omega_n = 34$ rad/s and a damping ratio $\zeta = 0.7$ were requested leading to the following values:

P–PI: $K_P = 24.3$, $K_V = 11.9$, $T_V = 0.017$.

P–P–PI: $K_P = 24.3$, $K_V = 68.6$, $K_A = 0.6$, $T_A = 0.017$.

Remarkably, with the P–P–PI controller it was possible to assign a disturbance rejection factor $X_R = 1000$, which is greater than that of the P–PI controller ($X_R = 289.17$). Furthermore, the state-variable filter, necessary to reconstruct both velocity and acceleration in the P–P–PI scheme, was designed to have a natural frequency $\omega_{nf} = 200\pi$ rad/s and a damping ratio $\zeta = 0.5$; also, the filter was implemented in discrete time at 1 ms to ensure a sampling frequency 10 times as much as the filter natural frequency.

A continuous-time analysis in the frequency domain, using the software package CC, was developed to investigate the stability of the P–P–PI scheme with and without the filter. The results are reported in Fig. 5.

The comparison of the two open-loop transfer functions (Fig. 5(a)) shows that the effect of the filter is a reduction of the stability margins, while the two closed-loop transfer functions (Fig. 5(b), (c)) do not differ appreciably in the bandwidth of interest ($\omega < 34$ rad/s). In detail, the phase margin is reduced to 36°, thus setting a constraint on the maximum time lag that can be tolerated in the loop (1.23 ms).

In view of discrete-time implementation, we expect that the chosen sampling time, as well as the parametric variation, precludes a further increase of the gains of the compensator (K_A in particular), being the system close to the stability limit. In any case, having good stability margins is always recommended to account for the occurrence of unmodeled effects.

A joint motion of π rad to be executed in a time of 0.1 s was assigned; the desired position trajectory (dashed line in the figures) was computed using a fifth-order polynomial that provides null values of initial and final velocities and accelerations.

In the first test, a unitary step disturbance torque was applied at 0.2 s; notice that the unitary value is quite strong, being 2 N · m the value of the nominal torque. The time history of the joint trajectories and relative errors show a drastic improvement of performance: for the P–P–PI scheme, a better disturbance rejection is obtained with respect to the P–PI scheme (Fig. 6(a), (b)), while the recovery time is the same, as expected.

In the second test, the disturbance torque was chosen as a sinusoidal signal with amplitude of 0.2 N · m and frequency of 10 rad/s to fall in the bandwidth of interest. The time history of the joint trajectories and relative errors confirm the anticipated conclusion that the performance improves as an extra feedback loop is nested around the disturbance (Fig. 6(c), (d)).

Notice that the imperfect tracking occurring also with feedforward action in Fig. 6 is purely caused by the artificial discrepancy introduced between the value of inertia used in simulation and that used for feedforward design. Noticeably, with regard to this effect, the P–P–PI scheme performs still better than the P–PI scheme.

V. Experimental Tests

In order to test the practical implementation of the proposed P–P–PI controller, the high-speed three-degree-of-freedom parallel robot DELTA [20] available at LIRMM was considered (Fig. 7). This robot has a traveling plate connected to the base plate by three kinematic chains actuated by PARVEX brushless motors. Each motor is equipped with a digital encoder whose resolution is 10 000 counts per revolution. It was exploited the possibility, offered by the motors' amplifiers, to control the currents. This prototype robot has the unique feature of having a lightweight structure. Then it might be argued that the nonlinear dynamic terms are negligible. However, the end-effector accelerations reach typical values as high as 10 g. This fact, together with the low value of gear ratios (1 : 10), produces appreciable coupling effects and then constitutes a good testbed for our control scheme.

A very fast three-Transputer system of INMOS T800's was utilized, whose boards were developed at LIRMM. One of the boards is used to implement the control algorithms and communicate with the host PC; the decod-

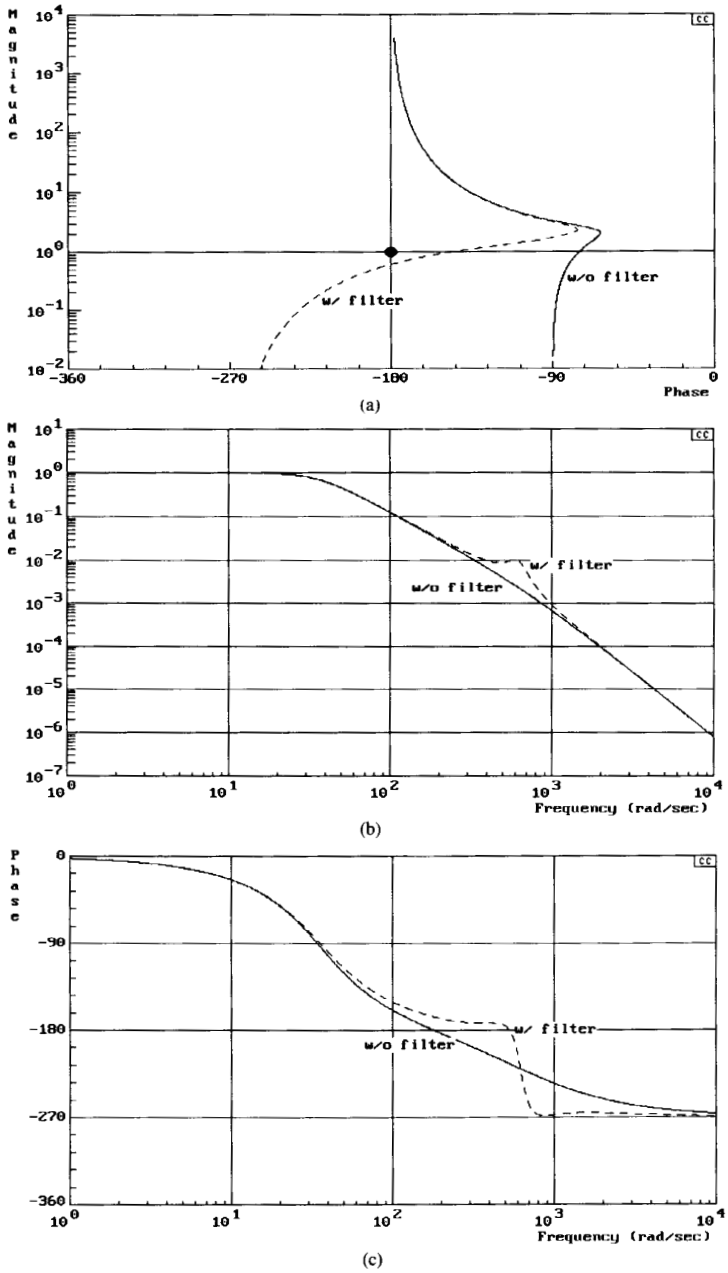

Fig. 5. Frequency plots for the P–P–PI scheme. (a) Nichols plot of open-loop transfer functions. (b) Bode magnitude plot of closed-loop transfer functions. (c) Bode phase plot of closed-loop transfer functions.

ing of joint encoders' measurements plus the reconstruction of both joint velocity and acceleration are performed on another transputer board; the third board is basically a D/A output board.

A rough identification process was performed: with only the arm connected to the motor via the gear transmission, the identified parameters of the linear model in (7) are $k_m = 837.7$ s/V and $T_m = 0.4$ s. Also, the presence of a static friction torque of 0.05 Nm was identified.

The design specs for the P–PI controller were $\omega_n = 62.8$ rad/s and $\zeta = 0.7$; the gains were computed via (10), (11), resulting in a disturbance rejection factor $X_R = 4.7$. On the other hand, different values of X_R were set for the P–P–PI controller and the relative gains were computed via (20)–(22). As for the state-variable filter used to reconstruct velocity and acceleration, $\omega_{nf} = 200\pi$ rad/s and $\zeta = 0.5$ were chosen to have good reconstruction. Both the controllers and the reconstructing filter were

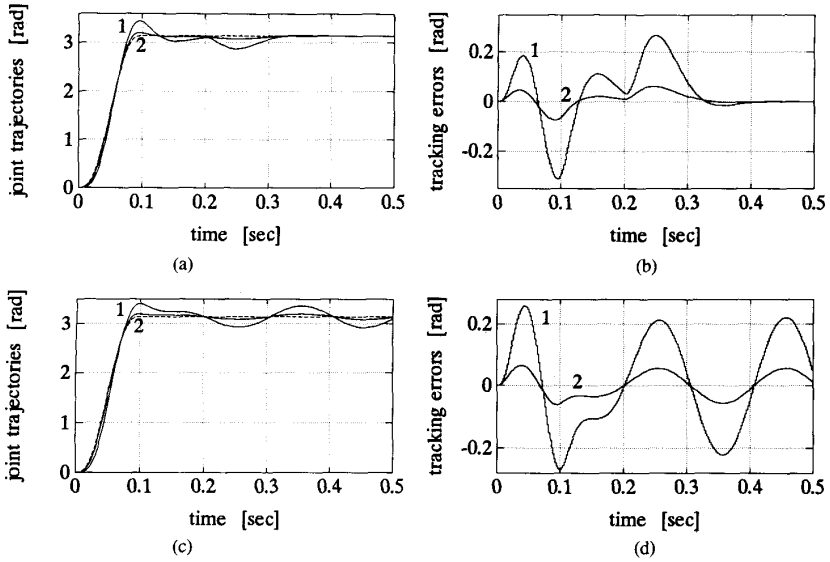

Fig. 6. Comparison of the P–PI scheme (1) and the P–P–PI scheme (2). (a) Time history of joint trajectories for a step disturbance torque. (b) Time history of tracking errors for a step disturbance torque. (c) Time history of joint trajectories for a sinusoidal disturbance torque. (d) Time history of tracking errors for a sinusoidal disturbance torque.

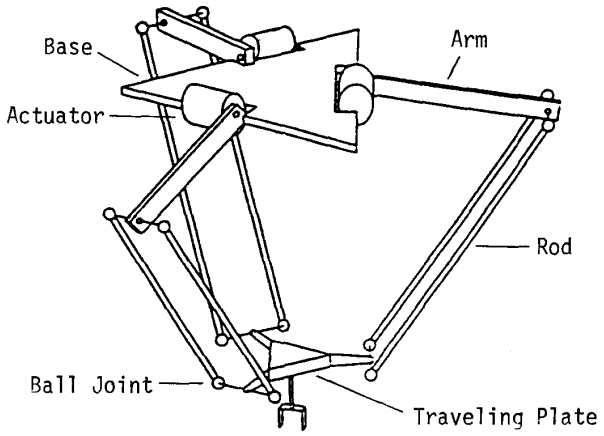

Fig. 7. The DELTA parallel robot.

converted in their discrete-time equivalent versions before implementation.

Two sets of experimental tests were performed. In the first set, only one motor with its arm connected via the gear transmission is controlled so that no dynamic coupling is present; the same conditions as for the above identification hold. In the second set, the whole robot was employed and the same controllers for the three motors with the same gains as above were used; this allows to evaluate the capability of rejecting the disturbance caused by dynamic coupling.

First, the two control schemes (P–PI and P–P–PI) were compared at a sampling time of 0.3 ms. For each test the following schemes were used: without feedforward (labeled 1 in the figures), with feedforward of static friction (label 2), with feedforward of velocity and velocity + acceleration (label 3), with both feedforward actions (label 4). In all trials, the same motor was moved of 5000 encoder counts using a fifth-order polynomial as the reference trajectory (dashed line in the figures); the motor starts and arrives at rest, and it reaches one half of the maximum allowable velocity and acceleration. This corresponds to a joint motion of 0.1π rad to be performed in 0.075 s, with a maximum velocity of 8 rad/s and a maximum acceleration of 340 rad/s^2; at the tip of the arm the resulting velocity is of 2 m/s and the acceleration of 88 m/s^2. These values cause nonnegligible dynamic effects, which can be recognized in the following experimental results.

Fig. 8(a), (b) show the obtained trajectories and tracking errors when the P–PI controller was used and only the arm was connected. Notice that the use of feedforward terms gives better results, since the system is in the same condition under which identification was carried out. In Fig. 8(c), (d) the same curves are plotted when the whole robot is running; it is quite evident to recognize the poor performance of the scheme. The errors are given in encoder counts; 100 counts correspond to 0.002π rad at the joint.

Next, the P–P–PI controller was applied under the same conditions. The disturbance rejection factor was $X_R = 10$; larger values lead to gains causing instability. In Fig. 9 the errors are plotted for the single arm (a) and the whole robot (b), respectively. It is clear that this scheme performs better than the P–PI scheme; the errors in both cases are as much as half of the previous ones—the rejection factor is now almost doubled.

In order to obtain higher disturbance rejection factors with the P–P–PI controller while preserving closed-loop

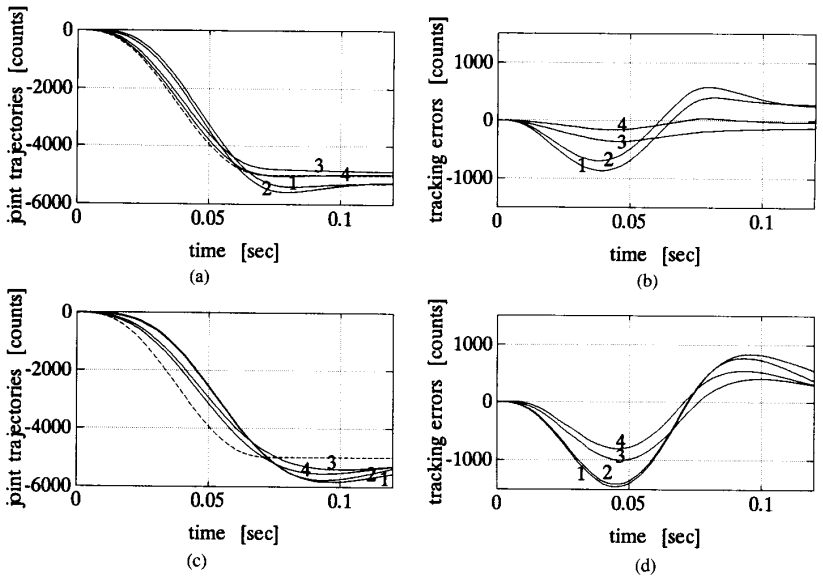

Fig. 8. P–PI scheme at a sampling time of 0.3 ms. (a) Time history of joint trajectories for the sole arm. (b) Time history of tracking errors for the sole arm. (c) Time history of joint trajectories for the whole robot. (d) Time history of tracking errors for the whole robot.

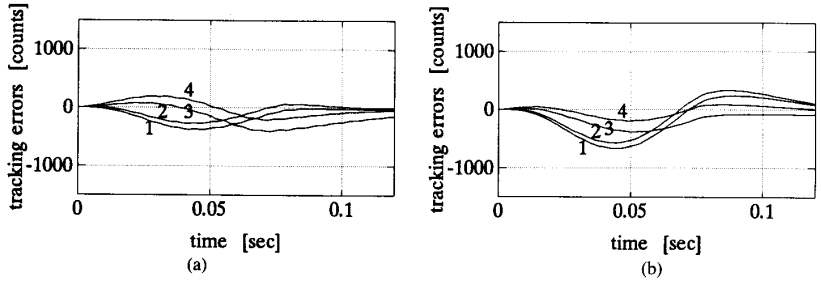

Fig. 9. Time history of tracking errors with the P–P–PI scheme at a sampling time of 0.3 ms. (a) Sole arm. (b) Whole robot.

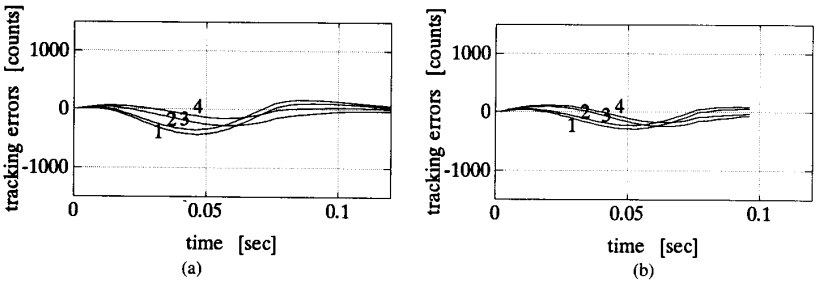

Fig. 10. Time history of tracking errors with the P–P–PI scheme for the whole robot at different sampling times. (a) 0.2 ms. (b) 0.16 ms.

system stability, it is necessary to decrease the sampling time. With a sampling time of 0.2 ms, it was possible to achieve $X_R = 15$. Figure 10(a) shows that tracking errors for the whole robot become smaller. Furthermore, with a sampling time of 0.16 ms, which is the minimum achievable with the current transputer system, it was obtained $X_R = 18$. The resulting errors for the whole robot are plotted in Fig. 10(b). In this case, it is worth noticing that there is no substantial difference on the tracking performance when feedforward is added; in fact, with such a

rejection factor, the P–P–PI controller does not need an accurate knowledge of the model. Nevertheless, it should be recalled that the feedforward actions are based only on a rough identification of the linearized model and of the static friction torque.

VI. Conclusions

A new robust independent joint control scheme with acceleration feedback was extensively tested both in simulations on a single-joint drive system and in experiments on a high-speed parallel robot. The obtained results confirmed the theoretical findings, i.e., closing an extra feedback loop around the disturbance input achieves better performance over the conventional PID scheme in terms of rejection factor and recovery time. The implementation problem of lack of direct joint acceleration measurements was solved by using a suitable state-variable filter. In conclusion, it is believed that the proposed control scheme represents a practical, valid alternative to model-based control schemes of second-order mechanical systems with highly coupled dynamics.

Acknowledgment

Helpful comments by an anonymous reviewer are thankfully acknowledged.

References

[1] R. M. Goor, "A new approach to minimum time robot control," in *Proc. 106th ASME Winter Annu. Meeting—Robotics and Manufacturing Automation*, Miami, FL, PED, vol. 15, 1985, pp. 1–11.

[2] R. P. C. Paul, "Modeling, trajectory calculation, and servoing of a computed controller arm," Memo. Am-177, Stanford AI Laboratory, Stanford University, Palo Alto, CA, 1972.

[3] A. K. Bejczy, "Robot arm dynamics and control," Jet Propulsion Lab., California Institute of Technology, Pasadena, CA, JPL Tech. Memo 33-669, 1974.

[4] J. J. Craig, *Introduction to Robotics: Mechanics and Control*, 2nd ed. Reading, MA: Addison-Wesley, 1989.

[5] J.-J. E. Slotine and W. Li, "On the adaptive control of robot manipulators," *Int. J. Robotics Res.*, vol. 6, no. 3, pp. 49–59, 1987.

[6] R. Ortega and M. W. Spong, "Adaptive motion control of rigid robots: A tutorial," *Automatica*, vol. 25, pp. 877–888, 1989.

[7] N. Sadegh and R. Horowitz, "Stability and robustness analysis of a class of adaptive controllers for robotic manipulators," *Int. J. Robotics Res.*, vol. 9, no. 3, pp. 74–92, 1990.

[8] H. Asada and K. Youcef-Toumi, *Direct-Drive Robots: Theory and Practice*. Cambridge, MA: MIT Press, 1987.

[9] P. K. Khosla and T. Kanade, "Experimental evaluation of nonlinear feedback and feedforward control schemes for manipulators," *Int. J. Robotics Res.*, vol. 7, no. 1, pp. 18–28, 1988.

[10] C. H. An, C. G. Atkeson, J. D. Griffiths, and J. M. Hollerbach, "Experimental evaluation of feed forward and computed torque control," *IEEE Trans. Robotics Automat.*, vol. 5, pp. 368–372, 1989.

[11] M. B. Leahy Jr. and G. N. Saridis, "Compensation of industrial manipulator dynamics," *Int. J. Robotics Res.*, vol. 8, no. 4, pp. 73–84, 1989.

[12] P. Chiacchio. L. Sciavicco, and B. Siciliano, "The potential of model-based control algorithms for improving industrial robot tracking performance," in *Proc. IEEE Int. Workshop on Intelligent Motion Control*, Istanbul, Turkey, 1990, pp. 831–836.

[13] M. B. Leahy Jr., "Compensation of industrial manipulator dynamics in the presence of variable payloads," *Int. J. Robotics Res.*, vol. 9, no. 4, pp. 86–98, 1990.

[14] M. B. Leahy Jr., "Model based control of industrial manipulators: An experimental analysis," *J. Robotic Sys.*, vol. 7, pp. 741–758, 1990.

[15] P. Chiacchio, L. Sciavicco, and B. Siciliano, "Practical design of independent joint controllers for industrial robot manipulators," in *Proc. 1992 American Control Conf.*, Chicago, IL, pp. 1239–1240, 1992.

[16] G. L. Luo and G. N. Saridis, "L–Q design of PID controllers for robot arms," *IEEE J. Robotics Automat.*, vol. RA-1, pp. 152–159, 1985.

[17] J. Studenny and P. Bélanger, "Robot manipulator control by acceleration feedback: Stability, design and performance issues," in *Proc. 25th IEEE Conf. on Decision and Control*, Athens, Greece, 1986, pp. 80–85.

[18] J. E. McInroy and G. N. Saridis, "Acceleration and torque feedback for robotic control: Experimental results," *J. Robotic Syst.*, vol. 7, pp. 813–832, 1990.

[19] T. C. S. Hsia, T. A. Lasky, and Z. Guo, "Robust independent joint controller design for industrial robot manipulators," *IEEE Trans. Ind. Electron.*, vol. 38, pp. 21–25, 1991.

[20] F. Pierrot, C. Reynaud, and A. Fournier, "DELTA: A simple and efficient parallel robot," *Robotica*, vol. 8, pp. 105–109, 1990.

[21] F. Pierrot, A. Fournier, and P. Dauchez, "Towards a fully-parallel 6 dof robot for high speed applications," in *Proc. 1991 IEEE Int. Conf. on Robotics and Automation*, Sacramento, CA, 1991, pp. 1288–1293.

Pasquale Chiacchio was born in Naples, Italy, on September 7, 1963. He received the Laurea and the Research Doctorate degrees from the University of Naples in 1987 and 1992, respectively, both in electronics engineering.

Since 1988 he has been working at the Department of Computer and Systems Engineering where he is currently a Research Associate. From June to December 1991 he was a Visiting Scholar at LIRMM, University of Montpellier, under an ESPRIT research grant. His research interests include manipulator inverse kinematics techniques, robot robust control, optimal control of redundant manipulators, and cooperative robot manipulation.

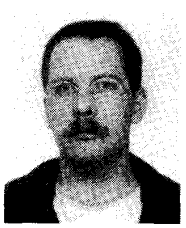

François Pierrot was born in Mont-Saint-Martin, France, on November 2, 1961. He received the Maîtrise degree and the Professeur Agrégé teaching diploma from the University of Paris in 1986 and 1987, respectively, both in mechanical engineering, and the Doctorate degree in robotics from the University of Montpellier, France, in 1991.

Since 1988 he has been with the University of Montpellier where he is currently a Research Associate at LIRMM, a research unit of the National Center for Scientific Research (CNRS). His research interests are in the areas of robots with complex architecture, multiarm and

parallel robots, high-speed robots, transputer-based controllers, and hybrid force/position control.

Lorenzo Sciavicco was born in Rome, Italy, on December 8, 1938. He received the Laurea degree in electronics engineering from the University of Rome in 1963.

Since 1970 he has been working at the Department of Computer and Systems Engineering at the University of Naples where he is currently Professor of Automatic Control. His research interests include automatic control theory and applications, manipulator inverse kinematics techniques, redundant manipulator control, cooperative robot manipulation, and force/position control of manipulators.

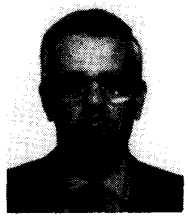

Bruno Siciliano (M'91) was born in Naples, Italy, on October 27, 1959. He received the Laurea and the Research Doctorate degrees from the University of Naples in 1982 and 1987, respectively, both in electronics engineering.

Since 1983 he has been working at the Department of Computer and Systems Engineering where he is currently Associate Professor of Industrial Robotics. From Fall 1985 to Spring 1986 he was a Visiting Scholar at the School of Mechanical Engineering of the Georgia Institute of Technology, Atlanta, GA, under a NATO research fellowship. His research interests include manipulator inverse kinematics techniques, modeling and control of lightweight flexible arms, redundant manipulator control, cooperative robot manipulation, force/position control of manipulators and output feedback control of two-time scale systems. He is a Technical Editor of the IEEE TRANSACTIONS ON ROBOTICS AND AUTOMATION.